Chemical Engineering Journal 164 (2010) 432–441

Contents lists available at ScienceDirect

Chemical Engineering Journal

journal homepage: www.elsevier.com/locate/cej

Numerical study of the effects of particle size and polydispersity on the agglomerate dispersion in a cyclonic flow

Z.B. Tong[a], R.Y. Yang[a,*], K.W. Chu[a], A.B. Yu[a], S. Adi[b], H.K. Chan[b]

[a] Laboratory for Simulation and Modelling of Particulate System, School of Materials Science and Engineering, University of New South Wales, Sydney, NSW 2052, Australia
[b] Faculty of Pharmacy, University of Sydney, NSW 2006, Australia

ARTICLE INFO

Article history:
Received 3 September 2009
Received in revised form
19 November 2009
Accepted 22 November 2009

Keywords:
Powder dispersion
Cyclonic flow
Inhaler
Agglomerates
Computational fluid dynamics
Discrete element method

ABSTRACT

This paper presents an investigation of powder dispersion based on a combined computational fluid dynamics (CFD) and discrete element method (DEM) approach. Agglomerates of different particle sizes and polydispersities are dispersed in a cyclonic flow at different flow velocities. The analysis of flow field and agglomerate properties indicates that the dispersion is governed by two competitive interactions, i.e. particle–particle cohesion and particle–wall impact, with the latter related to the air flow or the particle–fluid interaction. The internal shearing induced by air flow, however, only plays a minor role in powder dispersion for the system considered. The dispersion performance is described by fragment size distribution and fine particle fraction (FPF) which is the weight percentage of fragments with size less than 4.5 μm. Agglomerates of finer particles are more difficult to disperse at low flow rates due to strong particle–particle cohesion, but their dispersion becomes more efficient at high flow rates. Agglomerates with narrower particle size distributions tend to have better dispersion. An index based on the ratio of particle–wall impact energy and agglomerate cohesion energy is proposed to provide a quantitative characterization of dispersion performance.

1. Introduction

In recent years there has been high commercial interest in the pharmaceutical industry and biotechnology to develop dry powder aerosols for drug delivery to the respiratory tract for both local and systemic therapeutic effects [1,2]. Existing dry powder inhalers (DPIs) have low efficiency and high variability of dosing, and generally less than 30% of the dose loaded to the device will deposit in lungs [3]. This is due to the strong cohesion between fine particles which are usually less than 5 μm and hence are more difficult to disperse (or de-agglomerate).

To improve the aerosol performance, research in the past two decades has been focused on the formulation properties [3]. However, powder dispersion also depends strongly on particle characteristics (e.g. size and size distribution) and prevailing flow conditions inside an inhaler device [4–7]. For example, Chew and Chan [5] studied experimentally the dispersion of mannitol powder of different sizes at different air flow rates. Their results showed that the fine particle fractions (FPF), defined as the weight percentage of fragments with size less than 4.5 μm, increase with particle size at low flow rates. The relation between FPF and particle size, however, is reversed at high flow rates. They also observed that powder differed only in polydispersity (span) generate similar FPF, particularly at high flow rates [6]. Hence the effects of particle size, size distribution and flow rate should be considered simultaneously when optimising dispersion performance. So far the principal mechanisms leading to powder deagglomeration in inhalers remain unclear. Some work indicated that drag force generated by turbulent flow is a principal source of deagglomeration [8–10], while others suggested that separation force caused by mechanical impaction may also be important [8,11,12]. Experimentally, however, it is difficult to obtain detailed and quantitative information about the dispersion mechanisms due to the small size of agglomerates and the short duration of dispersion.

To develop an understanding of air flow and deagglomeration in inhaler devices, computational fluid dynamics (CFD) simulations have been performed [13–16]. The results showed that small variations in the device design (grid size, mouthpiece geometry, inlet air dimension, presence of a capsule, and air flow rate) produce significant variations in the aerosol performance. However, CFD model does not consider explicitly the contact between fluid, particles and boundary surfaces with respect to particle inertial and materials properties. Therefore, it is impossible to model the discrete flow characteristic of individual particles. Such limitation can be overcome by the so-called discrete element method (DEM) [17] which treats particle flow as an assembly of discrete particles and

* Corresponding author at: School of Materials Science and Engineering, Gate 14, Barker Street, Sydney, NSW 2052, Australia. Tel.: +61 2 9385 6787; fax: +61 2 9385 5956.
E-mail address: r.yang@unsw.edu.au (R.Y. Yang).

1385-8947/$ – see front matter © 2009 Elsevier B.V. All rights reserved.
doi:10.1016/j.cej.2009.11.027

computes the motion of individual particles separately according to Newton's second law of motion. The interactions between particles in the system as well as particles and device are determined based on the relatively well established contact mechanics. We recently carried out DEM studies on the formation and breakage of loose agglomerates [18,19]. Our results showed that the structure and strength of agglomerates change significantly with particle size. Upon impact with a wall, agglomerates show large plastic deformations before disintegrating into small fragments. While increasing impact velocity improves agglomerate breakage, a 45-degree impact angle provides the maximum breakage for a given velocity. A quantitative index based on the total impact energy was proposed to characterise the effects of impact velocity and angle. In those studies, however, air flow was not considered and only mono-sized particles were used.

This paper is therefore to develop a combined CFD-DEM model for powder dispersion, which allows the direct consideration of particle–particle, particle–fluid and particle–device interaction forces. A cyclonic flow model similar to the commercial Aeroliser® inhaler is chosen so that the numerical data can be compared with experimentally measured results. The effects of key variables associated with powder characteristics (i.e. size and size distribution) and operational condition (air flow rate) are investigated. Finally, an index based on the mechanical strength of agglomerates and particle–wall impact energy is proposed to characterise dispersion efficiency.

2. Model development and simulation condition

2.1. CFD-DEM model

The present work treats the dispersion process as a particle–fluid flow where the discrete particles and the continuous air flow are modelled by DEM and CFD, respectively. In DEM model, the translational and rotational motions of a particle in a system are governed by its interactions with neighbouring particles, walls and surrounding fluid, which can be described by Newton's second law of motion [20]:

$$m_i \frac{d\mathbf{v}_i}{dt} = \sum_{j=1}^{k_i} (\mathbf{f}_{cn,ij} + \mathbf{f}_{dn,ij} + \mathbf{f}_{ct,ij} + \mathbf{f}_{dt,ij} + \mathbf{f}_{v,ij}) + \mathbf{f}_{pf,i} + m_i\mathbf{g} \quad (1)$$

$$I_i \frac{d\boldsymbol{\omega}_i}{dt} = \sum_{j=1}^{k_i} (\boldsymbol{R}_i \times (\boldsymbol{f}_{ct,ij} + \boldsymbol{f}_{dt,ij}) - \mu_r |\boldsymbol{f}_{cn,ij}| \hat{\boldsymbol{\omega}}_i) \quad (2)$$

where m_i, I_i, $\mathbf{v}_i$, and $\boldsymbol{\omega}_i$ are, respectively, the mass, moment of inertia, translational and rotational velocities of particle i. $\mathbf{R}_i$ is the vector from the centre of particle i to a contact point. k_i is the number of particles contacting with particle i. μ_r is the rolling friction coefficient. $\hat{\boldsymbol{\omega}}_i = \boldsymbol{\omega}_i/|\boldsymbol{\omega}_i|$. The forces involved are the gravitational force, $m_i\mathbf{g}$, inter-particle forces between particles i and j, which include the normal and tangential contact forces $\mathbf{f}_{cn,ij}$ and $\mathbf{f}_{ct,ij}$, the viscous damping forces $\mathbf{f}_{dn,ij}$ and $\mathbf{f}_{dt,ij}$, the van der Waals force $\mathbf{f}_{v,ij}$, and the particle–fluid interaction force, $\mathbf{f}_{pf,i}$.

Table 1
Parameters used in the simulations.

Parameter	Value
Particle density, ρ_p	1490 kg m^{-3}
Young's modulus, Y	1×10^8 N m^{-2}
Poisson's ratio, $\tilde{\sigma}$	0.29
Sliding friction coefficient, μ_s	0.3
Rolling friction coefficient, μ_r	0.002
Normal damping coefficient, γ	2×10^{-6} s^{-1}
Hamaker constant, H_a	1.2×10^{-19} J

The governing equations for the continuous fluid in CFD model are the conservations of mass and momentum in terms of the local mean variables over a computational cell, given by [21–23]

$$\frac{\partial \varepsilon}{\partial t} + \nabla \cdot (\varepsilon \boldsymbol{u}) = 0 \quad (3)$$

$$\frac{\partial (\rho_f \varepsilon \tilde{\mathbf{u}})}{\partial t} + \nabla \cdot (\rho_f \varepsilon \overline{\mathbf{u}\mathbf{u}}) = -\nabla P - \boldsymbol{F}_{fp} + \nabla \cdot (\varepsilon \boldsymbol{\tau}) + \rho_f \varepsilon \mathbf{g} + \nabla \cdot (-\rho \overline{\mathbf{u}'\mathbf{u}'}) \quad (4)$$

where ε, $\tilde{\mathbf{u}}$, $\mathbf{u}'$, ρ_f, P and $\boldsymbol{\tau}$ are porosity, fluid mean velocity, turbulent velocity fluctuation, fluid density, pressure and fluid viscous stress tensor, respectively. The volumetric fluid–particles interaction force $\mathbf{F}_{fp}$ is define as $\sum_{i=1}^{k_c} \boldsymbol{f}_{pf,i}$, where k_c is the number of particles in a CFD cell. The Reynolds stress model (RSM) is used to solve the Reynolds stress term $-\rho\overline{\mathbf{u}'\mathbf{u}'}$ as this model is more accurate to describe swirl flow [24,25]. Detailed descriptions of the forces in Eqs. (1)–(4) can be found from [26,27]. Table 1 lists the parameters used in the simulations.

A one-way DEM-CFD coupling method was adopted in the simulations. Unlike a two-way coupling method which considers both particles to fluid and fluid to particles interactions and the momentums between particles and fluid are exchanged simultaneously, the current one-way method only considers the interaction of fluid on particles but ignores the reaction of particles on fluid. Such simplification is justified since the current work only considers the dispersion of single agglomerates. Both the agglomerates and the fragments generates are small

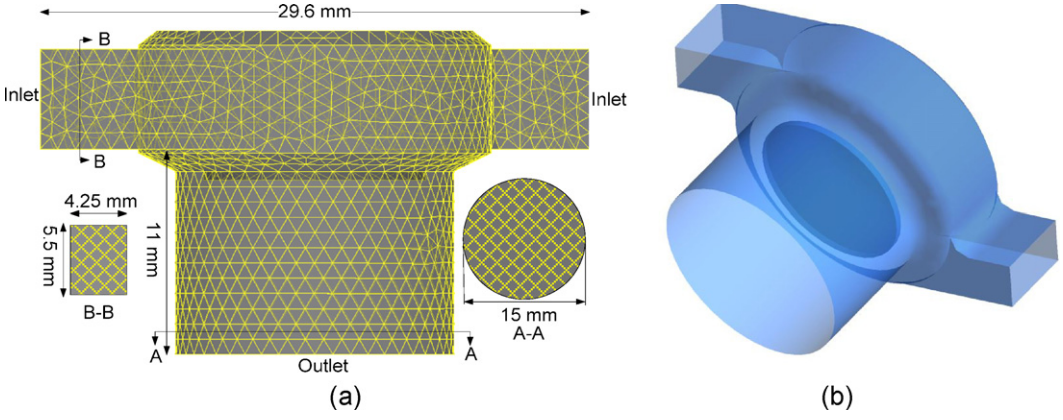

Fig. 1. (a) Schematic and numerical grid representation (A–A and B–B are inhaler outlet and inlets, respectively); and (b) three-dimensional view of the cyclonic model.

in volumes comparing to the fluid field. Therefore, the effect of the solid particles on the surrounding fluid is negligible. Our tests using both one-way and two-way coupling methods showed the simulation results quite comparable. The one-way coupling method, however, could speed up the simulations by 5 times. Therefore, the method is implemented in the simulation s as follows. The fluid flow is first solved using the commercial software Fluent® until the flow reaches a steady state. Then the fluid flow information (velocity and pressure in this case) is transferred to DEM model to calculate particle-related information, such as the positions and velocities of individual particles, and to determine porosity in the individual computational cells and particle–fluid interaction force on particle scale. Such process continues until the simulation finishes.

2.2. Simulation conditions

This work focuses on the dispersion process of single agglomerate in a cyclonic model which has two air inlets and one outlet, as shown in Fig. 1. In the simulation, an agglomerate is introduced via the left inlet with zero initial velocity while air flow enters from both inlets with a pre-set velocity. The agglomerate starts to accelerate due to the flow drag force and, due to flow shearing and turbulence and impact with the device, is dispersed into small fragments which are then discharged from the outlet.

The agglomerates are formed with mannitol powder under an assumed centripetal force as described in our previous work [18]. The particles in an agglomerate are bound by the cohesive van der Waals forces which are balanced by the contact forces between particles. Five agglomerates are generated using powders of different sizes and size distributions, as shown in Fig. 2. The particle size is represented by the mass median diameter D_{50}, and the particle polydispersity by span which is equal to $[D_{90} - D_{10}]/D_{50}$, where D_{90} and D_{10} are the equivalent mass diameters at 90% and 10% cumulative mass, respectively. Agglomerates A, B and E have similar spans with decreasing D_{50}, while agglomerates B, C and D have similar D_{50} with increasing span. Fig. 3 shows the morphology of the formed agglomerates, which have similar masses and sizes so their effects on dispersion are minimised. The representative structural and mechanical properties of the agglomerates are listed in Table 2. Note that $FPF_{original}$ is the amount of fine particles (defined as the weight percentage of particles/fragments with size less than 4.5 μm) in the original agglomerates. The tensile strength of an agglomerate is calculated by [18]:

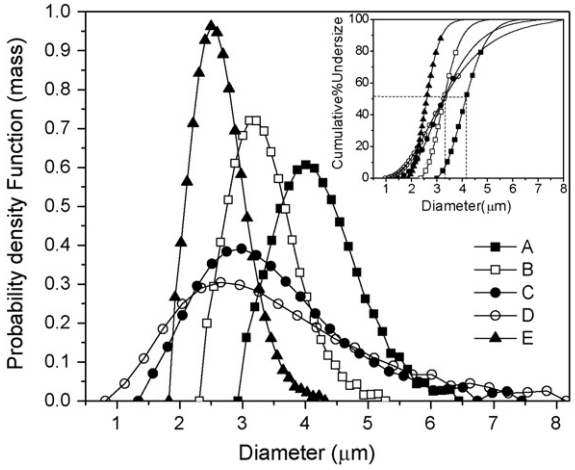

Fig. 2. Mass based size distribution of parimary powder. The inset shows the cumulative mass distribution.

Table 2
Properties of agglomerates.

	Agglomerate				
	A	B	C	D	E
Particle number	1000	2000	3000	4000	4000
D_{50} (μm)	4.142	3.277	3.274	3.273	2.603
Span	0.412	0.412	0.864	1.168	0.413
Diameter (μm)	50.44	51.06	51.12	51.36	52.78
Mass (mg)	0.497	0.496	0.501	0.479	0.491
Porosity	0.501	0.513	0.509	0.538	0.563
Tensile strength (Pa)	416.45	527.09	590.85	622.54	755.48
$FPF_{original}$	69%	97%	83%	77%	100%

$$\sigma_t = \frac{1}{3}\sigma_{ii} = \frac{1}{3V}\sum_{i}^{N} r_i \left(\sum_{j=1}^{z_i} \boldsymbol{n}_{ij} \cdot \boldsymbol{f}_{v,ij} \right) \quad (5)$$

where V is the volume of the agglomerate, N the total number of particles, r_i the particle radius, z_i the coordination number and $\mathbf{n}_{ij}$ the unit vector connecting the centres of particles i and j. It is observed that, with decreasing particle size (A → B → E), both tensile strength of the agglomerates and $FPF_{original}$ increase. On the other hand, increasing particle span (B → C → D) increases ten-

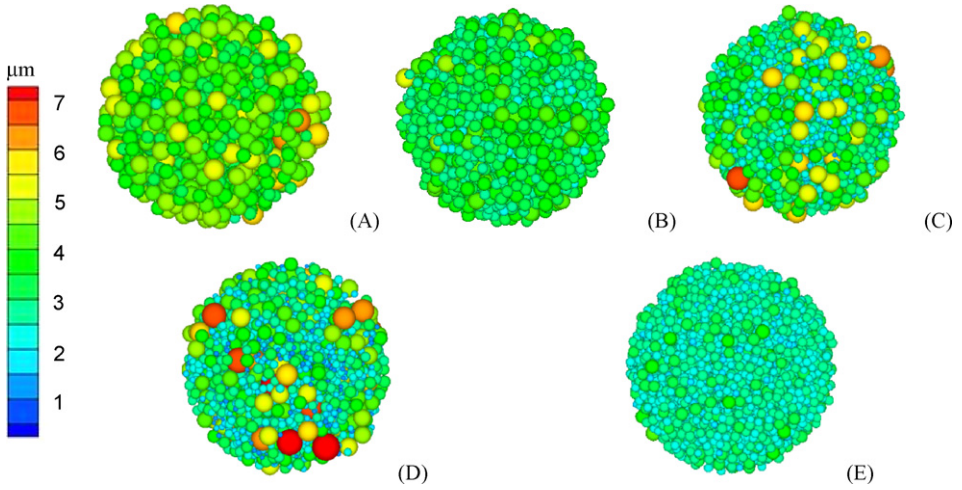

Fig. 3. Morphology of the formed agglomerates (the colours represent particle diameter). (For interpretation of the references to colour in this figure legend, the reader is referred to the web version of the article.)

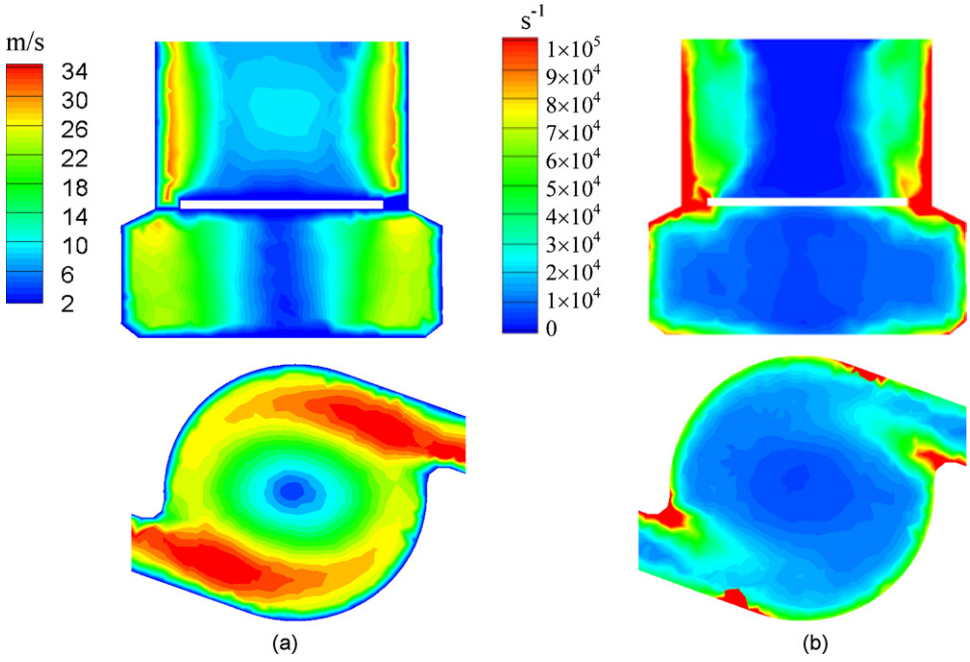

Fig. 4. Side and top views of (a) velocity; and (b) integral scale strain rate with flow velocity of $v = 30$ m/s.

sile strength but reduces $FPF_{original}$. Table 2 also shows that the variation of particle size has a larger effect on the agglomerate strength than particle span for the system considered in this work.

In the following sections, the flow properties and the dynamics of agglomerate dispersion will be discussed. It should be noted that this work only considers the dispersion of single agglomerate in which particle–wall impact and particle–fluid interactions are two mechanisms for dispersion. In reality with many agglomerates, the agglomerate–agglomerate impact may also play an important role which is ignored here but needs to be investigated in the future study.

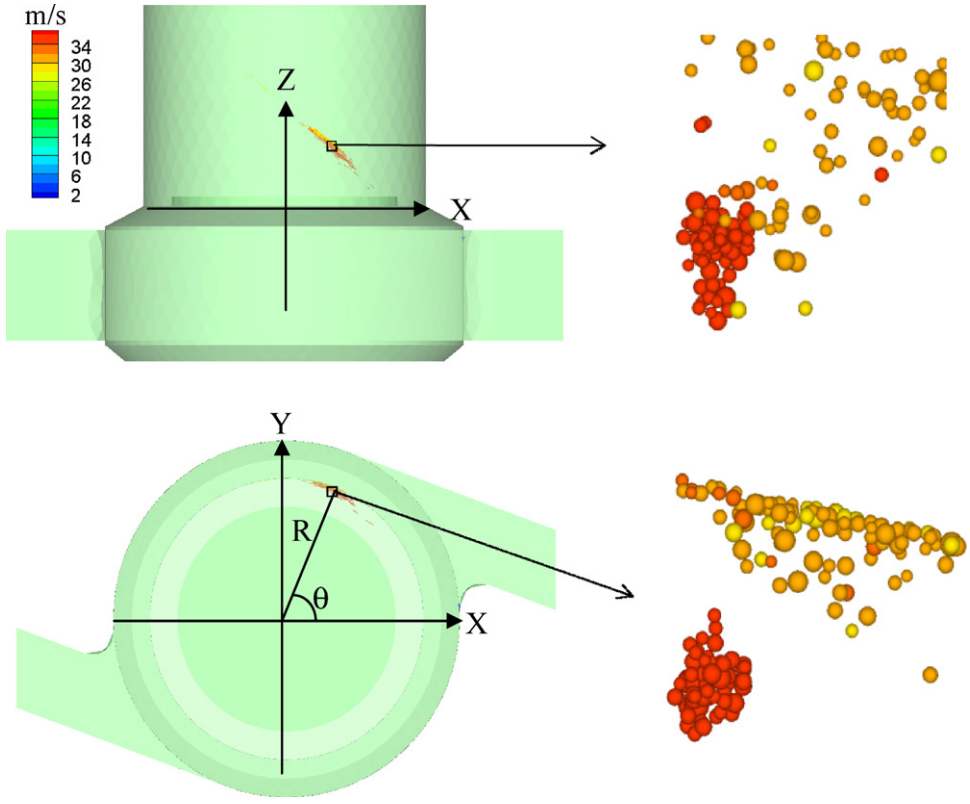

Fig. 5. The side (top) and top (bottom) views of particles velocity and breakage pattern of agglomerate B at $t = 0.0015$ s with air flow velocity $v = 30$ m/s. The angle θ represents the angle between the geometry centre of the agglomerate and the X-axis.

3. Results and discussion

3.1. Air flow pattern

This work investigates agglomerate dispersion at different flow velocities from 20 to 60 m/s (equivalent to flow rates of 55–165 L/min), which are typical values used in physical experiments [4,5]. Fig. 4 shows the flow field at the flow velocity of $v = 30$ m/s. Fig. 4a indicates a typical cyclonic flow pattern with the velocity having the maximum of 34 m/s near the two inlets, gradually slowing down along the flow direction and reaching the lowest velocity of 2 m/s at the centre. On the other hand, Fig. 4b shows that the integral scale strain rate, i.e. the turbulence dissipation rate divided by the turbulence kinetic energy, increases along the radial direction of the cyclonic model and has a maximum value at the neck of the cyclonic model. While the turbulence kinetic energy is a measure of the absolute turbulence level generated in the device, the integral scale strain rate is a measure of the velocity gradient across the integral scale eddies (the most energetic occurring in a turbulence flow) [11]. It has been demonstrated to be more relevant to agglomerate dispersion [28]. Other flow rates have similar spatial distributions and are therefore not shown here.

In the one-way coupling simulations as used in the current work, flow field depends only on flow rate and does not change during dispersion for a given flow rate. Therefore, our discussions in the following sections will mainly focus on the analysis on the discrete particles. The dynamic behaviour of agglomerates in the inhaler will be examined first, followed by the analysis of fragments discharged from the outlet.

3.2. Dynamics of dispersion

Fig. 5 shows the velocity and breakage pattern of agglomerate B at the flow velocity $v = 30$ m/s. The snapshot is taken at $t = 0.0015$ s when the agglomerate breaks into small fragments due to the impact with the wall. Fig. 6 shows that increasing flow velocity decreases the agglomerate residence time t_e which is defined as the duration of the agglomerate in the device before being discharged from the outlet. Our simulations suggest that the residence time t_e for all agglomerates has a linear relation with the reciprocal of flow velocity. Since a larger span or D_{50} generates larger fragments, t_e increases slightly with span (B → C → D) or D_{50} (E → B → A).

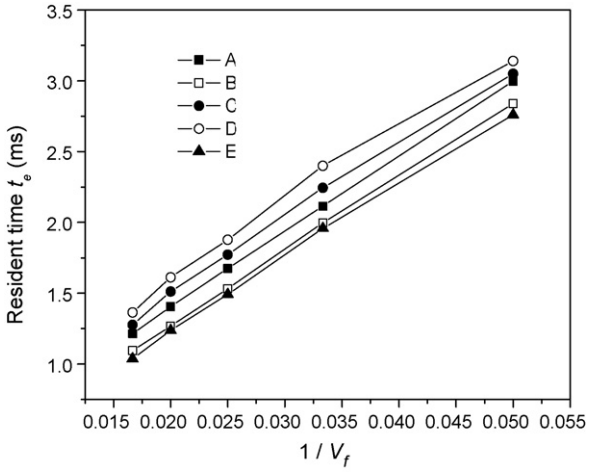

Fig. 6. Residence time t_e as a function of the reciprocal of flow velocity.

Micro-dynamic analysis is a particle scale analysis including the trajectories and the transient forces of the particles in an agglomerate. It can be made by following the flow path of the agglomerate based on the dynamic information from simulations. Such information is important to understand the underlying mechanisms. A cylindrical coordinate system, as shown in Fig. 5, is set up to determine the position of an agglomerate, in which Z, R, θ are the vertical, radial and angular coordinates, respectively. Here the position of an agglomerate is represented by the geometrical centre of the agglomerate which is the average of the coordinates of all the constituent particles. A piece of fragment is defined as an assembly of particles which are bound together but are separate from other particles. Fig. 7 shows some representative results for agglomerate B dispersed at different flow velocities. Figs. 7a–c show the position of the agglomerate centre at the radial, vertical and angular directions. When plotted against the time normalised by the residence time, the trajectories of the agglomerate at different flow velocities are very similar except for the slight difference in the radial direction. This indicates that the agglomerate largely follows the flow path line. Fig. 7d shows that the average velocities of the agglomerate also have similar patterns although they increase with flow velocity. Fig. 7e plots the particle–wall interaction during the dispersion process.

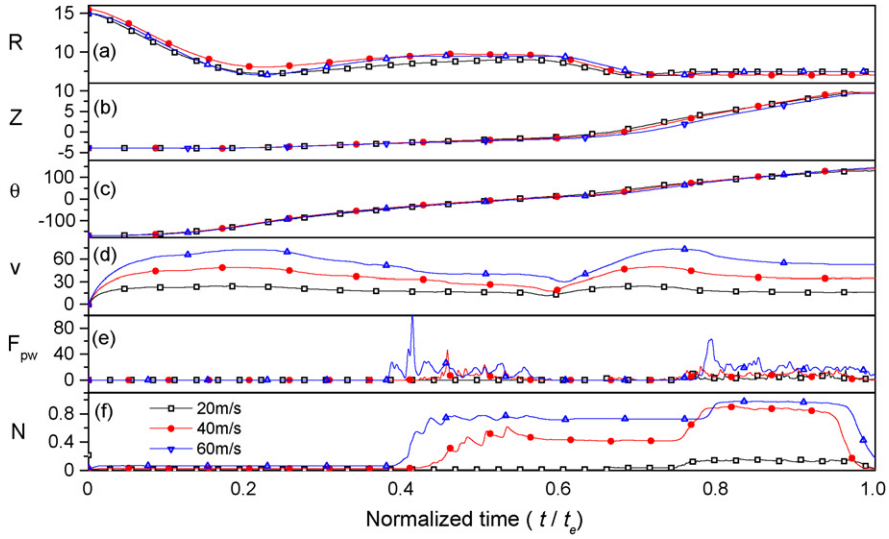

Fig. 7. Time evolution of the dynamic properties of agglomerate B at different flow velocities: (a)–(c) the geometry centre of agglomerate in the radial, vertical and angular directions; (d) average velocity of particles (m/s); (e) particle–wall contact force (μN); and (f) fragment number normalised by the number of particles.

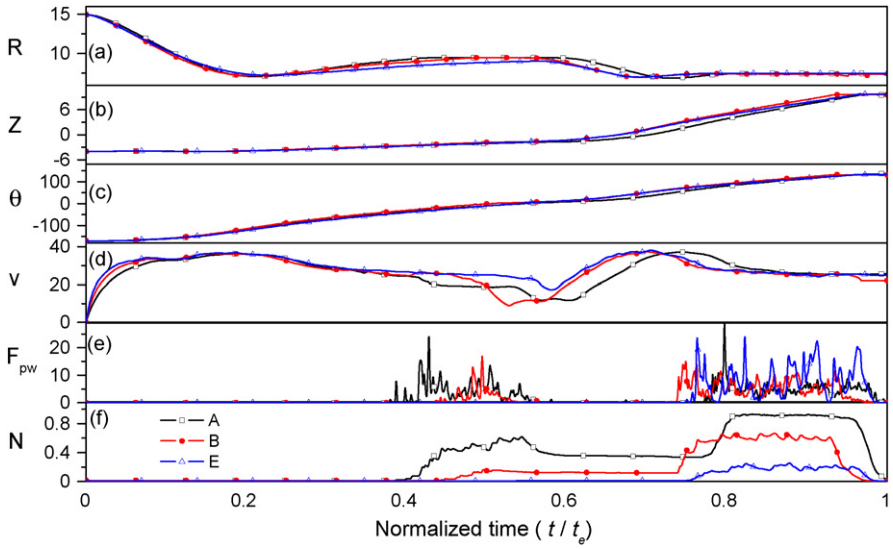

Fig. 8. Time evolution of the dynamic properties of agglomerates A, B and E at $v = 30$ m/s: (a)–(c) the geometry centre of agglomerate in the radial, vertical and angular directions; (d) average velocity of particles (m/s); (e) particle–wall contact force (μN); and (f) fragment number normalised by the number of particles.

At the low velocity of 20 m/s, agglomerate B has only one impact with the wall at around 0.75 (t/t_e). At the higher velocities of 40 and 60 m/s, two agglomerate–wall impacts occur at t around 0.4 (t/t_e) and 0.8 (t/t_e), thus generating more fragments as shown in Fig. 7f. After each impact, there is a sharp increase in the number of fragments. With increasing velocity, the agglomerate–wall impact force (intensity) increases, which also produces more fragments. This indicates that agglomerate breakage is closely linked to agglomerate–wall impact.

Fig. 8 shows the effects of particle size on the dispersion process by examining the dispersion behaviour of agglomerates A, B and E at the flow velocity of $v = 30$ m/s. Again, the trajectories of the three agglomerates are similar when plotted against the normalised time (Fig. 8a–c), which suggests that their movements are largely driven by fluid flow. Their velocity profiles are also similar before impacting on the wall (Fig. 8d). Before moving to the vertical tube ($Z > 0$) at the time of 0.65 (t/t_e), agglomerate A has an impact from 0.38 (t/t_e) to 0.55 (t/t_e) as shown in Fig. 8e. The first impact for agglomerate B occurs slightly later from 0.43 (t/t_e) to 0.56 (t/t_e) and there is no impact for agglomerate E before it moves to the vertical pipe. All three agglomerates have an impact with the vertical wall from 0.73 (t/t_e) to 0.98 (t/t_e). Correspondingly, the number of fragments increases sharply after impacts (Fig. 8f). As agglomerate E has only one impact, its fragment number is the least. While both agglomerates A and B have two impacts, agglomerate A with larger D_{50} produces more fragments due to reduced particle–particle cohesion.

Fig. 9 compares the behaviours of agglomerates B, C and D which have different spans. Their trajectories and velocities are similar before impacting on the wall. The first impact for the three agglomerates occurs from 0.38 (t/t_e) to 0.56 (t/t_e). The second impact occurs in the vertical tube, and is stronger and lasts longer than the first one. Although the particle–wall impact force has similar magnitudes for the agglomerates, agglomerate B generates more fragments than others due to smaller tensile strength. However, comparing Fig. 8f with Fig. 9f reveals the differences in the number of fragments caused by span being smaller than those by particle size. The above analysis indicates that particle–wall impact energy

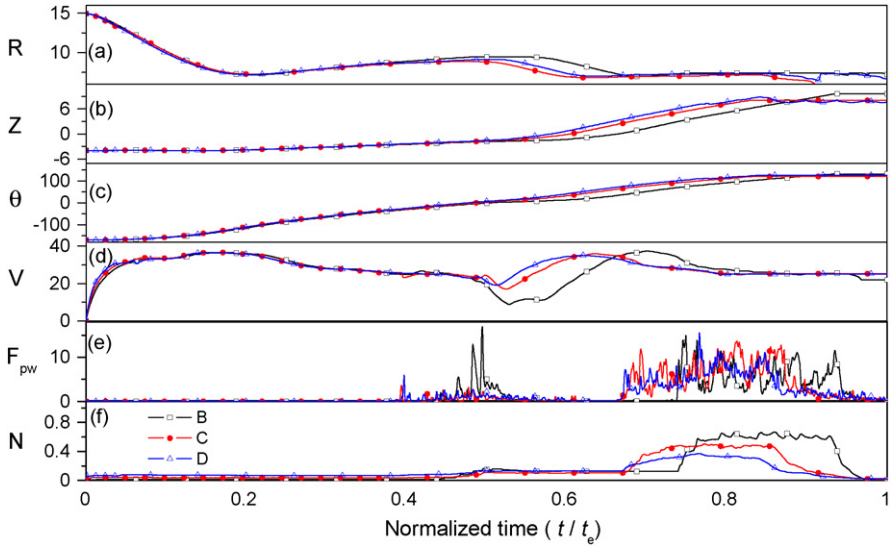

Fig. 9. Time evolution of the dynamic properties of agglomerates B, C and D at $v = 30$ m/s: (a)–(c) the geometry centre of agglomerate in the radial, vertical and angular directions; (d) average velocity of particles (m/s); (e) particle–wall contact force (μN); and (f) fragment number normalised by the number of particles.

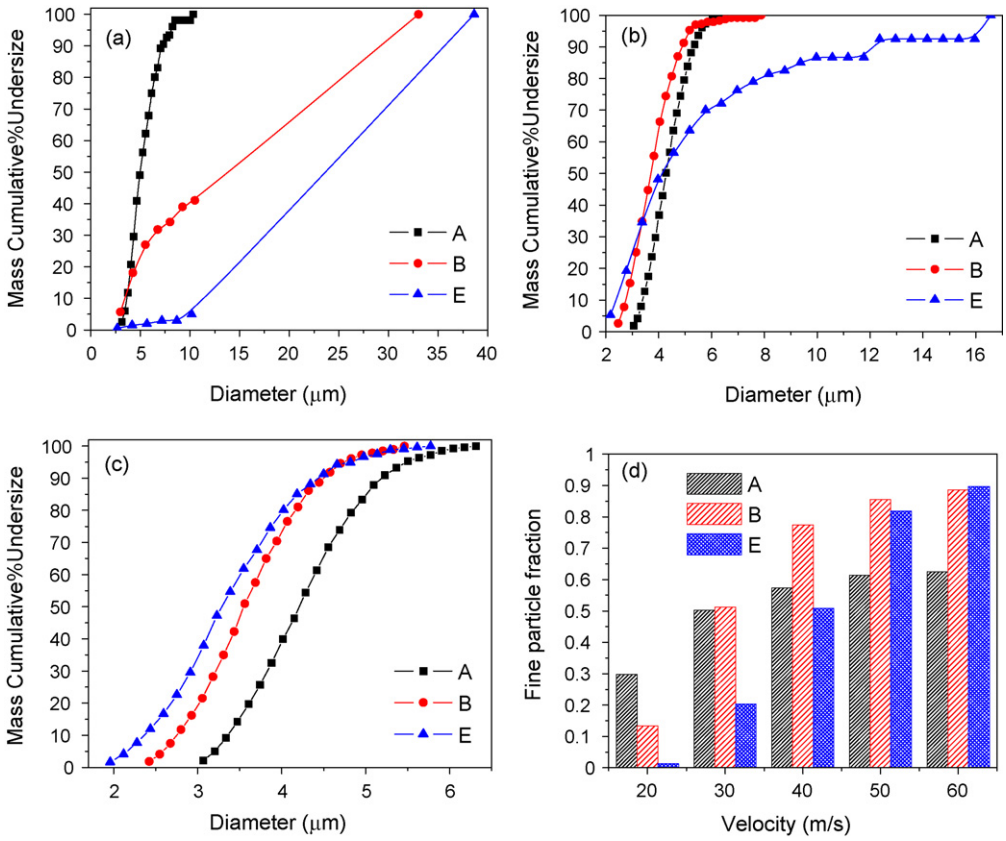

Fig. 10. Comparisons of the size distribution of fragments at different flow velocities: (a) 20 m/s; (b) 40 m/s; (c) 60 m/s; and (d) FPF after dispersion at different flow velocities.

and particle–particle tensile strength are two dominant factors in the breakage of agglomerates.

3.3. Post-impact analysis

This section is to quantitatively characterise the fragment size and dispersion efficiency of agglomerates, focusing on the combined effects of particle size and polydispersity with flow rate. The dispersion efficiency is characterised in terms of the FPF discharged from the outlet. An effort will also be made to quantify these effects.

3.3.1. Effect of particle size

Agglomerates A, B and E have similar spans with decreasing D_{50}. Fig. 10a–c show the cumulative size distribution of fragments at different flow velocities. At the low flow velocity of 20 m/s (Fig. 10a), the fragments size distribution curve of the agglomerate A (D_{50} = 4.1 μm) locates above those of agglomerates B and E across the whole size range except at very small size, indicating that the larger powder provides a better dispersion performance at the low flow velocity. While the fragments of agglomerate A show a relatively smooth size distribution, a sudden jump at the size of 10 μm for agglomerates B and E indicates that the two agglomerates have large fragments discharged from the outlet. As flow velocity increases to 40 m/s, agglomerate B has the best overall dispersion (Fig. 10b). Agglomerate E outperforms agglomerate A only for the fragments less than 4.5 μm. With the flow velocity increasing to 60 m/s, the fragment size curve of agglomerate E is situated above others, indicating a better dispersion (Fig. 10c). The smooth distribution curves suggest that the agglomerates are almost fully dispersed and a further increase in the flow velocity may not increase the dispersion efficiency.

Fig. 10d shows the FPF of the agglomerates at various flow velocities. In general, larger flow velocities generate larger FPFs for an agglomerate. However, different agglomerates behave differently with flow rates. While agglomerate A has the best dispersion efficiency at the low flow velocity of 20 m/s, agglomerates B and E generate more fine particles at the median and high flow rates, respectively. This is because although agglomerates formed with smaller particles are more cohesive, they also contain more fine particles than those formed with coarser particles. The particle–wall impact generated at low flow rates is not strong enough to overcome the particle–particle cohesion, thus giving lower dispersion efficiency. With increasing flow rate, the particle–wall impact becomes sufficient to break cohesions among smaller particles and thus releases more fine particles. Therefore, the FPF of smaller particles increases faster with flow rate, resulting in a reversal of the FPF trend at high flow velocities. Such phenomenon was also observed in the experiments [5]. In the experiments, mannitol powder differed only in the median particle size (2.5, 5.0 and 7.3 μm) were dispersed with different flow rates. The results showed that at a low flow rate of 30 L/min the FPF of the 2.7 μm powders is smaller than those of 5.0 and 7.3 μm powders, but at air flow rate larger than 60 L/min the FPF of 2.7 μm powders is larger than those of the other two sized powders.

3.3.2. Effect of polydispersity

Agglomerates B, C and D have different spans but similar D_{50}. Fig. 11a–c plots their cumulative size distributions at various flow velocities. At the low flow rate of 20 m/s (Fig. 11a), the aerosol curve for agglomerate B with span of 0.41 is slightly above other two curves for size less than 10 μm while agglomerate C has the poorest dispersion. The step changes of the distribution curves indicate poor dispersion process with large fragments discharged from the outlet. At the flow velocity of 40 m/s, the aerosol curves for the three agglomerates cross at 4.2 μm, as shown in Fig. 11b. Increasing flow velocity to 60 m/s moves the cross-point of aerosol curves

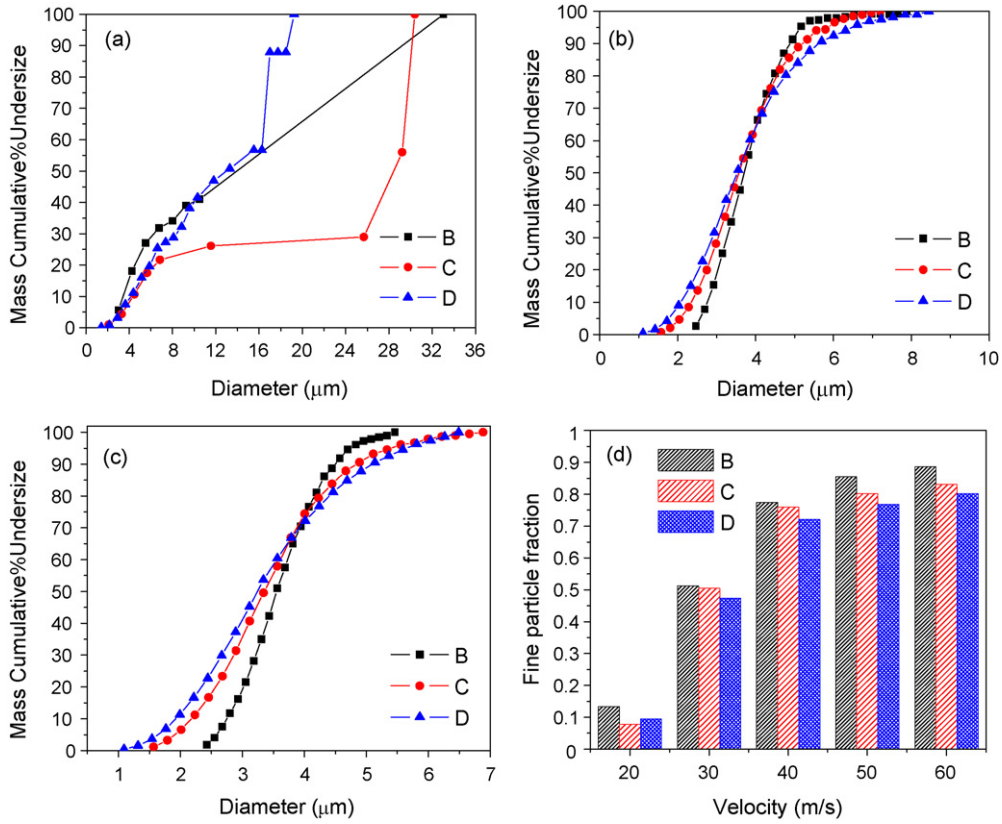

Fig. 11. Comparisons of the size distribution of fragments at different flow velocities: (a) 20 m/s; (b) 40 m/s; (c) 60 m/s; and (d) FPF after dispersion at different flow velocities.

to 3.8 μm. All three figures indicate that agglomerate B has better dispersion efficiency. This can also be confirmed in Fig. 11d which shows the agglomerates with smaller span (narrower size distribution) have larger FPF. However, the differences in FPF for the three agglomerates are very small, indicating that the effect of powder polydispersity on dispersion efficiency is less significant than particle size. One possible reason is because the change of span in our study is relatively small and thus the formed agglomerates have smaller difference in strength, as shown in Table 1. On the other hand, the current simulation results are consistent with the previous experimental observation [6]. In the experiments two mannitol powders differed only in spans were dispersed with various flow rates. When the flow rate is below 90 L/min, the FPF of the span 1.7 powders is slightly less than that of the span 1.1 powders. At the large flow rate of larger than 90 L/min, the FPF of the two powders are almost the same.

3.3.3. Dispersion mechanisms

As demonstrated above, agglomerate breakage is mainly determined by particle–particle cohesion and particle–wall impact. Since the particle–wall impact is governed by the particle–fluid interaction related to flow velocity, the effect of flow rate can also be reflected from the impact interactions. Therefore, establishing a quantitative link between the interaction forces and dispersion performance can provide a way to characterise and optimise dispersion processes based on simulation results.

By analysing the energy exerted from wall to agglomerates, our previous work [19] suggested that agglomerate breakage can be characterised in terms of total particle–wall impact energy E_{pw}, given by

$$E_{pw} = \sum_{i}^{k} \left[\int_0^t (v_{i,n} \cdot \boldsymbol{F}_{i,n}) \mathrm{d}t + \int_0^t (v_{i,t} \cdot \boldsymbol{F}_{i,t}) \mathrm{d}t \right] \quad (6)$$

where k is the number of particles impacting on the wall, and $\mathbf{F}_{i,n}$, $\mathbf{F}_{i,t}$, $\mathbf{v}_{i,n}$ and $\mathbf{v}_{i,t}$ are the forces and velocities of particle i in the normal and tangential directions, respectively. The summation is applied to all the particles which have contacts with the wall. t is the total impact time. Fig. 12a shows the variations of relative FPF (rFPF) with impact energy for all agglomerates. Here the FPF is normalized by the percentage of fine particles in the original agglomerate so the effect of initial FPF is minimised. As expected, rFPF increases with impact energy. However, the correlation is scattered since different agglomerates have different cohesion energies, which should also be considered. Here the cohesion energy of an agglomerate is defined as [18]

$$E_{ad} = \sum_{i}^{N} r_i \left(\sum_{j=1}^{z_i} \boldsymbol{n}_{ij} \cdot \boldsymbol{F}_{ij} \right) \quad (7)$$

where N is the number of particles in the agglomerate, r_i the radius of particle i, z_i the number of neighbouring particles of particle i, and $\mathbf{n}_{ij}$ the unit vector connecting the centres of particles i and j. The cohesion energy is similar to tensile strength and agglomerates with larger tensile strength have larger cohesion energy if the agglomerate sizes are similar. Fig. 12b plots rFPF as a function of the ratio of the impact energy and agglomerate cohesion energy. It is shown that the correlation for all agglomerates collapses into a single curve, indicating that agglomerate breakage is governed by the two competitive mechanisms. Dispersion has very low efficiency at small energy ratios (e.g. large agglomerate cohesion energy with small impact energy due to low flow velocity), but dispersion efficiency first increases rapidly with the energy ratio and then levels off at the energy ratio ϕ of around 3. A too large energy ratio has no obvious effect on the dispersion efficiency. It is observed that the correlation between the dispersion efficiency and the energy ratio

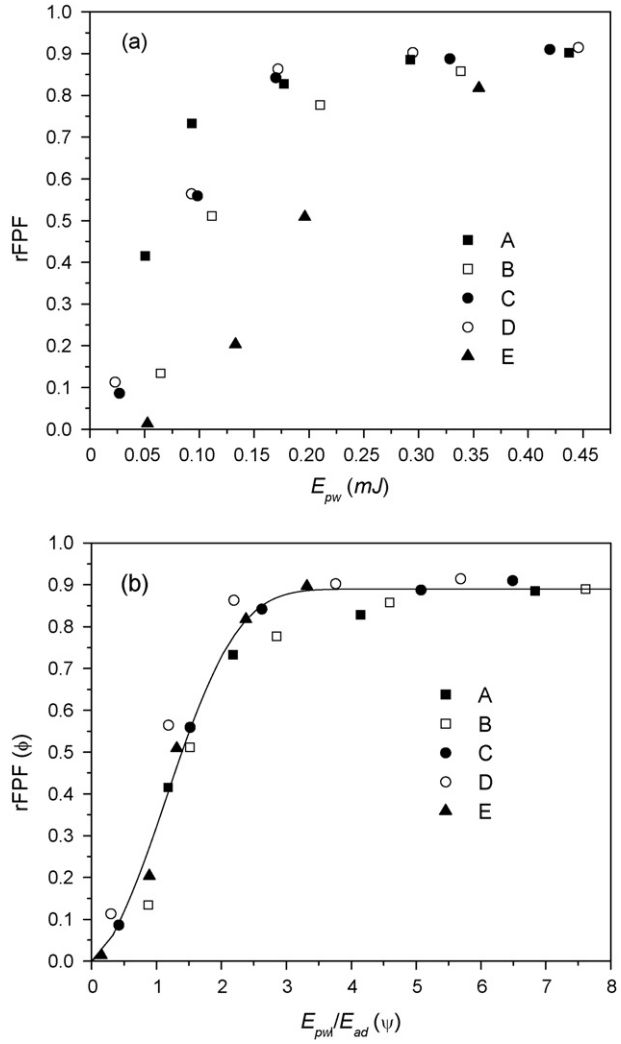

Fig. 12. Correlation between relative fine particle fraction (rFPF) and (a) particle–wall impact energy; and (b) the ratio of particle–wall impact energy and agglomerate cohesion energy. The line is the correlated curves by Eq. (8) with $\phi_\infty = 0.889$, $k = 1/3$ and $n = 3/2$.

can be fitted by the following equation:

$$\phi = \phi_\infty \, erf\,(k\psi^n) \tag{8}$$

where *erf*( ) is the error function, ϕ_∞ is the limiting rFPF when the energy ratio ψ is infinitely large, k and n are two empirical parameters. With the current results, $\phi_\infty = 0.889$, $k = 1/3$ and $n = 3/2$. Note that the cohesion energy is related to powder material properties and agglomerate structure, while the particle–wall impact energy is mainly controlled by the particle–fluid interaction or air flow as demonstrated above. Our results (Figs. 7–9) also suggest that the internal shearing induced by air flow is not important to powder dispersion in the device considered.

The above analysis shows that the ratio of impact energy and cohesion energy of agglomerates is a very useful parameter to characterise dispersion efficiency of fine powder agglomerate in inhalers. The results also demonstrate that the CFD-DEM based microscopic study can be linked to macroscopic process performance. Therefore, numerical simulations can be carried out to understand the actual dispersion behaviour in real devices. With fast advancement of computing capability, this technique has potential to reduce laborious experiments. To achieve this, however, more systematic studies are necessary in order to generalize this approach.

4. Conclusions

The powder dispersion in a cyclonic flow was simulated by a coupled CFD-DEM model. The flow field and the dynamic behaviour of agglomerates in the dispersion were examined. The effects of particle size and size distribution on dispersion efficiency in terms of fragment size and FPF were investigated. The results showed:

- The model can simulate effectively the dispersion process and the simulated results are qualitatively comparable with physical observations. The cyclonic air flow has the maximum velocity near the two inlets and the minimal at the centre. Agglomerates, whose motions are largely driven by the fluid–particle interaction, have impacts with the device wall, resulting in significant increases in the number of fragments.
- Particle size plays a significant role in the overall dispersion performance. While an agglomerates of smaller particles is more difficult to disperse at a low flow velocity, its dispersion becomes more efficient with increasing flow velocity and generates more fine particles. On the other hand, particles with a narrower size distribution have better dispersion, but the effect of size distribution is less significant than particle size for the systems considered, particularly at a high flow velocity.
- Powder dispersion mechanisms in the current model are governed by two competitive interactions: particle–wall impact and particle–particle cohesion. The internal shearing induced by air flow is not important to powder dispersion in the device considered. The dispersion efficiency can be correlated to the ratio of impact energy and cohesion energy. All the data obtained in the simulations fall into a single curve. The results indicate that the energy ratio, obtained from particle scale simulation, can be a useful index to predict dispersion performance at the macroscopic scale.

Acknowledgement

Authors are grateful to the Australia Research Council (ARC) for the financial support for this work.

References

[1] A.R. Clark, Pulmonary delivery technology: recent advances and potential for the new millennium, in: A.J. Hickey (Ed.), Drugs and the Pharmaceutical Sciences, Marcel Dekker, Inc., New York, 2004, pp. 571–591.
[2] J. Patton, Breathing life into protein drugs, Nat. Biotechnol. 16 (1998) 141–143.
[3] H.K. Chan, Dry powder aerosol delivery systems: current and future research directions, J. Aerosol Med.-Deposit. Clear. Effects Lung 19 (2006) 21–27.
[4] N.Y.K. Chew, D.F. Bagster, H.K. Chan, Effect of particle size, air flow and inhaler device on the aerosolisation of disodium cromoglycate powders, Int. J. Pharm. 206 (2000) 75–83.
[5] N.Y.K. Chew, H.K. Chan, Influence of particle size, air flow, and inhaler device on the dispersion of mannitol powders as aerosols, Pharm. Res. 16 (1999) 1098–1103.
[6] N.Y.K. Chew, H.K. Chan, Effect of powder polydispersity on aerosol generation, J. Pharm. Pharm. Sci. 5 (2002) 162–168.
[7] M.D. Louey, M. Van Oort, A.J. Hickey, Aerosol dispersion of respirable particles in narrow size distributions produced by jet-milling and spray-drying techniques, Pharm. Res. 21 (2004) 1200–1206.
[8] C.A. Dunbar, A.J. Hickey, P. Holder, Dispersion and characterization of pharmaceutical dry powder aerosols, KONA 16 (1998) 7–45.
[9] D.L. French, D.A. Edwards, R.W. Niven, The influence of formulation on emission, deaggregation and deposition of dry powders for inhalation, J. Aerosol Sci. 27 (1996) 769–783.
[10] W.-I. Li, M. Perzl, J. Heyder, R. Langer, J.D. Brain, K.H. Englmeier, et al., Aerodynamics and aerosol particle deaggregation phenomena in model oral-pharyngeal cavities, J. Aerosol Sci. 27 (1996) 1269–1286.
[11] W.H. Finlay, The Mechanics of Inhaled Pharmaceutical Aerosols, An Introduction, Academic Press, London, 2001.
[12] A. Voss, W.H. Finlay, Deagglomeration of dry powder pharmaceutical aerosols, Int. J. Pharm. 248 (2002) 39–50.
[13] E.A. Matida, W.H. Finlay, A. Rimkus, B. Grgic, C.F. Lange, A new add-on spacer design concept for dry-powder inhalers, J. Aerosol Sci. 35 (2004) 823–833.

[14] M.S. Coates, D.F. Fletcher, H.-K. Chan, J.A. Raper, Effect of design on the performance of a dry powder inhaler using computational fluid dynamics. Part 1. Grid structure and mouthpiece length, J. Pharm. Sci. 93 (2004) 2863–2876.
[15] M. Coates, H.-K. Chan, D. Fletcher, J. Raper, The role of capsule on the performance of a dry powder inhaler using computational and experimental analyses, Pharm. Res. 22 (2005) 923–932.
[16] E.A. Matida, W.H. DeHaan, W.H. Finlay, C.F. Lange, Simulation of particle deposition in an idealized mouth with different small diameter inlets, Aerosol Sci. Technol. 37 (2003) 924–932.
[17] P.A. Cundall, O.D.L. Strack, A discrete numerical model for granular assemblies, Geotechnique 29 (1979) 47.
[18] R.Y. Yang, A.B. Yu, S.K. Choi, M.S. Coates, H.K. Chan, Agglomeration of fine particles subjected to centripetal compaction, Powder Technol. 184 (2008) 122–129.
[19] Z.B. Tong, R.Y. Yang, A.B. Yu, S. Adi, H.K. Chan, Numerical modelling of the breakage of loose agglomerates of fine particles, Powder Technol. 196 (2009) 213–221.
[20] H.P. Zhu, Z.Y. Zhou, R.Y. Yang, A.B. Yu, Discrete particle simulation of particulate systems: theoretical developments, Chem. Eng. Sci. 62 (2007) 3378–3396.
[21] T.B. Anderson, R. Jackson, A fluid mechanical description of fluidized beds, Ind. Eng. Chem. Res. 6 (1967) 527.
[22] Y.Q. Feng, A.B. Yu, Assessment of model formulations in the discrete particle simulation of gas–solid flow, Ind. Eng. Chem. Res. 43 (2004) 8378–8390.
[23] D. Gidaspow, Multiphase Flow and Fluidization, Academic Press, San Diego, 1994.
[24] B. Wang, D.L. Xu, K.W. Chu, A.B. Yu, Numerical study of gas–solid flow in a cyclone separator, Appl. Math. Model. 30 (2006) 1326–1342.
[25] B.E. Launder, G.J. Reece, W. Rodi, Progress in development of a Reynolds-stress turbulence closure, J. Fluid Mech. 68 (1975) 537–566.
[26] K.W. Chu, B. Wang, A.B. Yu, A. Vince, CFD-DEM modelling of multiphase flow in dense medium cyclones, Powder Technol. 193 (2009) 235–247.
[27] R.Y. Yang, R.P. Zou, A.B. Yu, Computer simulation of the packing of fine particles, Phys. Rev. E 62 (2000) 3900–3908.
[28] M.S. Coates, H.K. Chan, D.F. Fletcher, J.A. Raper, Influence of air flow on the performance of a dry powder inhaler using computational and experimental analyses, Pharm. Res. 22 (2005) 1445–1453.